Polymer Vol. 37 No. 7, pp. 1243–1256, 1996

0032-3861/96/$15.00+0.00

Simulation of poly(phenylene oxide) reactors

Sanjay Kuberkar and Santosh K. Gupta*
Department of Chemical Engineering, Indian Institute of Technology, Kanpur 208016, India
(Received 12 April 1994; revised 4 July 1995)

A detailed kinetic model is developed for the polymerization of poly(phenylene oxide) (PPO). The Box complex technique is used to obtain the best-fit values of the parameters of the model (rate constants), using experimental data on the variation of the number-average chain length (μ_n) with time for one set of conditions. A sensitivity study helps to simplify this kinetic scheme. The Box complex method gives the optimal values of the four rate constants associated with this simplified model. The model is able to explain the two interesting features of this polymerization, namely: (i) a slow increase in μ_n with time during the initial period, followed by a sharp increase for a short duration; and (ii) a decrease in the polydispersity index at some intermediate time, associated with the mixing of several polymeric species having different individual chain-length distributions. The kinetic model can be adapted for use for simulating industrial PPO reactors wherein additional physical phenomena like heat and mass transfer are present.

(Keywords: poly(phenylene oxide); kinetics; reactor simulation)

INTRODUCTION

In recent years, thermoplastics have gained considerable popularity as engineering materials. One of the more important among these is poly(phenylene oxide) (PPO), commercially available as Noryl. This is a high-molecular-weight polymer that has excellent thermal and mechanical properties. Its glass transition temperature[1] is 205–210°C and it decomposes at relatively high temperatures (approx. 400°C). The backbone of the phenyl rings in the polymer chain imparts high mechanical strength to the polymer even at as low a temperature[2] as ≈200°C. These properties, combined with its high compatibility, easy processability and glossy look, make PPO very attractive for several applications.

Several studies have been reported in the open literature on the polymerization and the properties of PPO. These have formed the subject of three reviews[3–5]. Hay *et al.*[6] first reported the formation of high-molecular-weight poly(phenylene ether)s by the catalytic oxidation of the monomer, 2,6-disubstituted phenol, in solution, with oxygen gas bubbled through it. They also reported the formation of a waste by-product, diphenoquinone, in small quantities during polymerization. They later reported[7] work on the polymerization of monomers having different substituents. They observed that bulky groups such as t-butyl on the 2,6-disubstituted phenol produced larger quantities of diphenoquinone. On the other hand, methyl or ethyl groups produced high-molecular-weight polymers. Electronegative substituents, if present in the monomer, reduced the extent of polymerization. They also found that amine complexes of a copper salt are effective catalysts for the polymerization reaction. The ratio of amine to copper plays a crucial role in determining the final products of reaction.

Endres and Kwiatek[8] showed with experimental evidence that oxidation of 2,6-dimethylphenol in the presence of copper(I) chloride catalyst gives polymer following the step-growth mechanism. The main reaction is analogous to bifunctional polycondensation. A study of the rates of oxygen absorption in the polymerization of monomer, dimer, trimer and an intermediate polymer showed little dependence on the degree of polymerization. This indicates that the equal-reactivity hypothesis is applicable.

Endres *et al.*[9] have shown that formation of high-molecular-weight polymer and by-product diphenoquinone are competing reactions in the oxidation of 2,6-dimethylphenol. They showed that the rates of these reactions are very sensitive to reaction conditions, especially the Cu/ligand ratio. They also reported that increased temperature favours the formation of diphenoquinone. Finkbeiner *et al.*[10] studied the role of oxygen in this polymerization. They observed that the sole function of oxygen in the catalyst system is to reoxidize copper(I) to copper(II). Copper(II) is, thus, the true oxidizing agent in the oxidative coupling reaction. They reported formation of a copper–ligand complex, which actually catalyses the reaction. A similar study was carried out by McNelis[11] to determine the role of oxygen. He used MnO_2 as the oxidizing agent instead of gaseous oxygen. Similar results to those of the earlier studies were obtained. He suggested a quinol ether mechanism for the polymerization.

Several detailed mechanisms have been proposed for the oxidative coupling polymerization[3], including those involving ionic intermediates and free radicals. Tsuchida *et al.*[12] proposed a Michaelis–Menten type of model to

* To whom correspondence should be addressed

describe the kinetics of this polymerization. Mobley[13] proposed an improved model to account for catalyst deactivation during polymerization and for the difference in reactivity between monomer and all other oligomers. In these experiments, the rate of oxygen consumption was used as a measure of the rate of reaction. Recent studies[14,15] on PPO focus on the use of copper complexes of immobilized polymer-bound ligands, such as 4-(*N*,*N*-dimethylamino)pyridine, for the oxidative coupling of disubstituted phenols. These provide higher catalytic activity and better specificity for PPO formation.

So far, however, no significant efforts have been made towards modelling of the reaction and reactor system for PPO production. In view of the recent trend towards optimization and control of polymerization reactors, modelling of these reactors assumes considerable importance. In this study, we first develop a detailed model for the simulation of PPO reaction kinetics. We represent the reaction mechanism in a generalized manner incorporating the most important reactions and solve the mass-balance and moment equations using appropriate[16-18] closure conditions. The Box[19] complex method is used to curve-fit some experimental μ_n vs. t data[8] available in the open literature. A sensitivity study is then done on these parameters to identify the most important reactions in the kinetic scheme. It is observed that the reaction system is sensitive to only four parameters of the detailed model. The detailed kinetic scheme is simplified using this information. The parameters of the simplified model so developed are again curve-fitted. The simplified kinetic scheme developed here is well suited for use for the simulation of industrial PPO reactors wherein additional physical effects (e.g. vaporization, heat transfer, mass transfer, etc.) are present, as well as for their on-line control and optimization.

FORMULATION

Mechanism of 2,6-dimethylphenol polymerization

The chemical formula of PPO is:

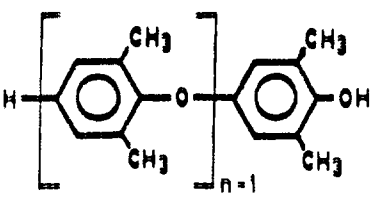

where n varies from 1 to about 250. The monomer of PPO is 2,6-dimethylphenol (2,6-DMP):

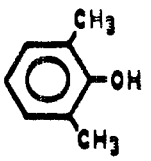

PPO is formed when 2,6-dimethylphenol in solution is polymerized in the presence of a copper catalyst. The reaction takes place by the oxidative coupling of 2,6-dimethylphenol. The oxidizing agent for coupling is molecular oxygen, supplied to the reactor system either by sparging oxygen or by using some oxidizing agent like MnO_2. The reaction requires a copper catalyst, which is usually a halide salt of copper, such as copper(I) chloride. An amine ligand is used, which binds the copper catalyst and facilitates polymerization. The most popular ligand is pyridine, the presence of which obviates the need for removal of the water of reaction from the reactor because of steric hindrance by its bulky phenyl ring. This prevents deactivation of the catalyst. The solvent used is normally toluene, but use of pyridine itself as a solvent has also been reported.

The currently accepted mechanism of polymerization of 2,6-dimethylphenol has been presented by Aycock *et al.*[3]. This, unfortunately, is not in a form amenable for use in reactor modelling studies. We have rearranged this scheme so as to facilitate the kinetic modelling of reactions of species of arbitrary length. The side reaction leading to the formation of diphenoquinone is not considered in this study because of the very small quantities formed under industrially relevant conditions. Seven reactions have been considered in this detailed scheme, and these are given in *Scheme 1*. In reaction 1, the copper(I)–pyridine complex is oxidized to copper(II)–pyridine complex. In reaction 2a, this activated complex reacts with the monomer to produce an intermediate species, which decomposes irreversibly to form an aryloxy radical, while regenerating the copper(I)–pyridine complex. A similar reaction with the Cu(II)–pyridine complex and higher-molecular-weight PPO molecules can also occur (reaction 2b) to generate aryloxy oligoradicals. In reaction 3, an aryloxy oligoradical reacts reversibly with an aryloxy monoradical to produce a quinol ether molecule. The latter can undergo irreversible intramolecular rearrangement (enolization) by reaction 4 to form a PPO molecule. Reactions 2–4 together impart some kind of chain-growth character to this polymerization, since the chain length effectively increases by one 'ring' at a time. Two more reactions take place, which involve quinone ketal formation. This species is formed by reaction 5 of *Scheme 1* from two polymeric radicals (or one monoradical and one macroradical). The quinone ketal so formed can decompose to radicals by the reverse reaction. The radicals can be either the same as or entirely different from the two radicals from which the quinone ketal molecule was originally formed. There is also an intramolecular shift of the cyclohexadiene group from left to right or from right to left in the quinone ketal molecule. This is shown as reaction 6. The shift of the cyclohexadiene group to either the right or left and its subsequent break-up by the reverse step of reaction 5 leads to the formation of high-molecular-weight macroradicals, which combine (by the forward step of reaction 5) to produce high-chain-length molecules. One special case of reaction 6 is that associated with the shift of the group to one end of the chain. The repeat unit at the end of the chain then gets converted to a quinol ether, as shown in reaction 7 of *Scheme 1*. Reactions 4–7 effectively impart a step-growth character to PPO polymerization because they involve the joining together of two macromers.

The rate constants indicated in *Scheme 1* are those associated with single sites. We must use appropriate

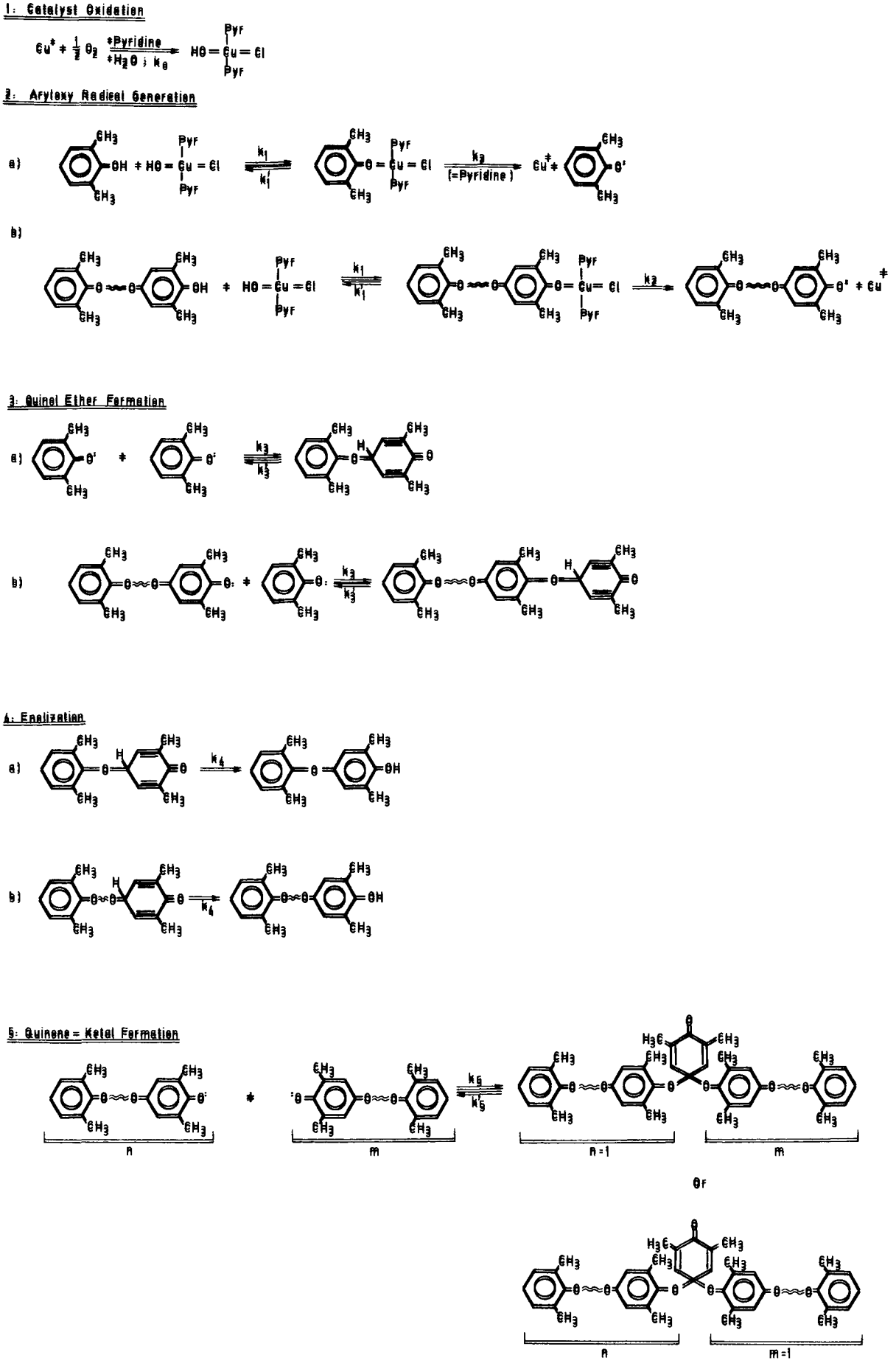

Scheme 1 Detailed reactions for PPO polymerization

6: Intermolecular rearrangement of Quinone Ketal

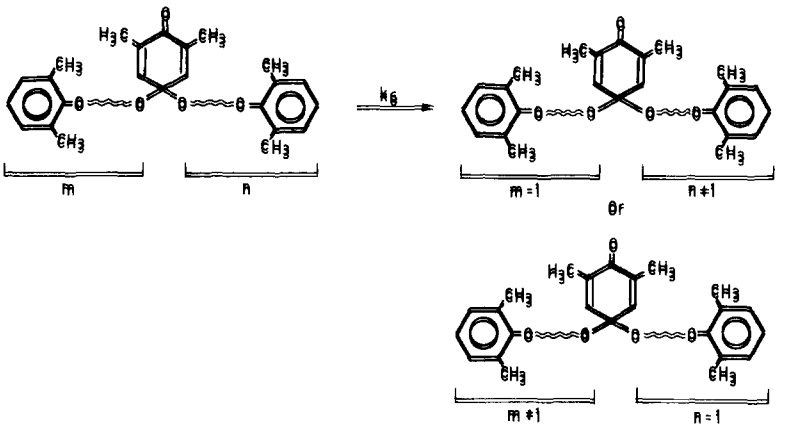

7: Special case of Reaction 6

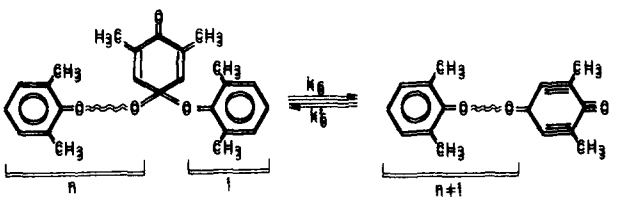

Scheme 1 continued

multiplying factors to account for the several possibilities of reaction between individual molecules[16]. In reaction 6, the rate constant associated with the shift in either direction is shown as k_6. In reaction 7, the forward step is associated with the same rate constant, k_6, since the rearrangements of the electrons are quite similar. However, the mechanism of formation of a quinol ether group is quite different, and the rate constant associated with the reverse step is written as k_6'.

In order to proceed further, we define several species in *Scheme 2*. The chain length n of any molecule reflects the number of 'rings' on that molecule. *Table 1* shows the various reactions of *Scheme 1* in terms of these species. The representation in this table is well suited for analysis

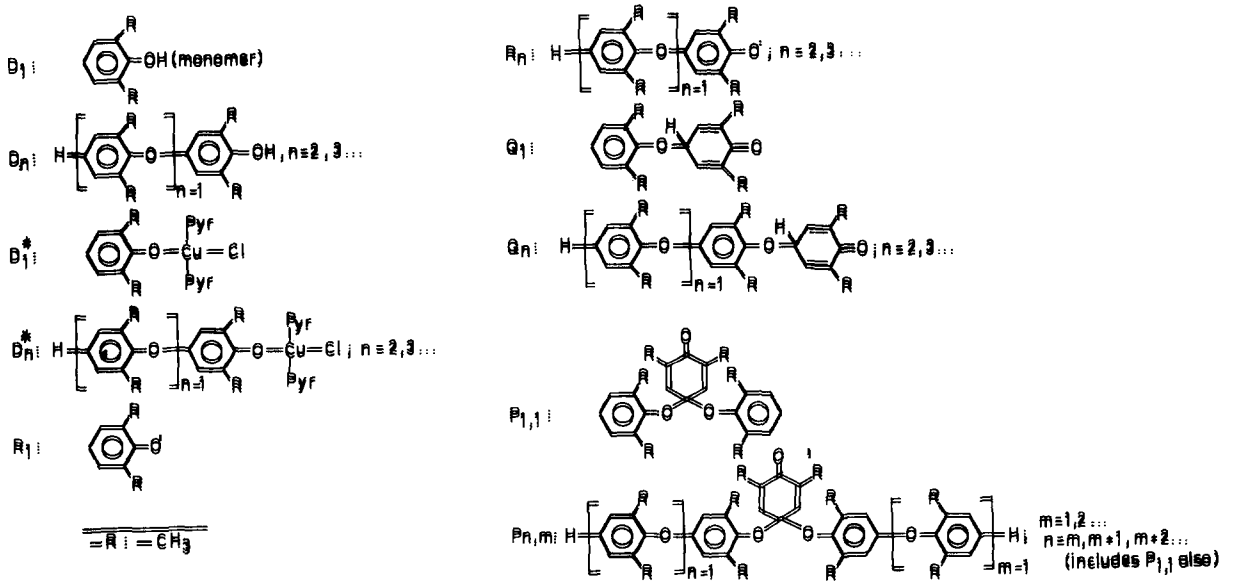

Scheme 2 Definition of various species for this study

Table 1 Kinetic scheme for 2,6-DMP polymerization

1. Catalyst oxidation

$$Cu^{+} + \tfrac{1}{2}O_2 \xrightarrow[k_0]{\text{pyridine, } H_2O} Cu^{2+}$$

2. Aryloxy radical generation

$$D_n + Cu^{2+} \underset{k_1'}{\overset{k_1}{\rightleftharpoons}} D_n^{*} \xrightarrow{k_2} R_n + Cu^{+} \qquad n = 1, 2, 3, \ldots$$

3. Quinol ether formation

$$R_n + R_1 \underset{k_3'}{\overset{k_3}{\rightleftharpoons}} Q_n \qquad n = 1, 2, 3, \ldots$$

4. Enolization

$$Q_n \xrightarrow{k_4} D_{n+1} \qquad n = 1, 2, 3, \ldots$$

5. Quinone ketal formation

$$R_n + R_m \underset{k_5'}{\overset{k_5}{\rightleftharpoons}} P_{n,m-1} \text{ or } P_{n-1,m}$$

$$m = 1, 2, 3, \ldots$$
$$n = m, m+1, m+2, \ldots \quad (\text{except } m = n = 1)$$

6. Intramolecular rearrangement of quinone ketal

$$P_{n,m} \underset{k_6}{\overset{k_6}{\rightleftharpoons}} P_{n+1,m-1} \text{ or } P_{n-1,m+1} \qquad \text{all independent possibilities}$$

7. Special case of reaction 6

$$P_{n,1} \underset{k_6'}{\overset{k_6}{\rightleftharpoons}} Q_{n+1} \qquad n = 1, 2, 3, \ldots$$

using conventional methods in polymer reaction engineering[16,17].

Mass-balance equations

The equations describing the variation of the concentrations of the various species present in a (well mixed batch) reactor can be written, with some effort, using the schematic reactions in *Table 1*. The final mass-balance equations are given in *Table 2*. While deriving these equations, extreme care has been taken to count the total number of ways in which the several sites on the reacting molecules can react. Also, we have studied the detailed electronic rearrangements taking place during reaction to achieve simplifications. A few examples indicate *some* of these details. The reaction between two aryloxy radicals always takes place in a head-to-tail manner, where the head is the oxygen end of the radical. Thus, there are two ways in which two aryloxy radicals can react. The multiplying factor of 2 with k_5 in the fifth term of equation (2.5) accounts for this multiplicity. The multiplying factor of 2 in the fifth term of equation (2.6) can also be explained similarly. When a reactant decomposes to produce two products, the number of different ways in which it can decompose is similarly considered. For example, in reaction 5 of *Table 1*, we find that $P_{n,m}$ can decompose in two different ways to produce either R_{m-1} and R_{n+1}, or R_{m+1} and R_{n-1}. This fact is accounted for in the third term of equation (2.21), as well as in the other equations for the quinone ketal species. In the intramolecular rearrangement of the quinone ketal species (reaction 6 in *Table 1*), it can be observed that the cyclohexadiene group can move to the right or the left with equal probability. Hence, from $P_{n,m}$ both $P_{n+1,m-1}$ and $P_{n-1,m+1}$ can be formed. This is reflected in the multiplying factor of 2 with k_6 in the fourth term of equation (2.21). This is, however, not true for some specific cases like intramolecular rearrangement of $P_{m+1,m}$. In this particular case, the movement of the cyclohexadiene group to the right produces $P_{m+1,m}$ and so, in effect, this reaction can be omitted. Only the shift to the left, which produces $P_{m+2,m-1}$, needs to be accounted for. Hence, the multiplying factor is unity in the fourth term of equation (2.19). Similarly, in the case of $P_{2,1}$, reaction 6 of the mechanism shown in *Table 1* does not take place since the shift of the cyclohexadiene group to the right produces $P_{2,1}$ again, while the shift to the left generates Q_3, which has been considered in reaction 7 of the mechanism. These and several similar details lead finally to the set of equations in *Table 2* (detailed derivation enumerating the possibilities can be supplied on request). To the best of our knowledge this is the first time that such a comprehensive scheme for PPO with its associated mass-balance equations has been presented in the open literature.

A well established method of solving the infinite set of coupled mass-balance equations is to use the method of moments[16,17]. Several workers have studied polymeric reactions in the past using this technique. The various moments used in this study involving the several species (and the number-average chain length, μ_n) are defined by:

$$\mu_k = \sum_{n=1}^{\infty} n^k [D_n] \tag{1}$$

$$\mu_k^{*} = \sum_{n=1}^{\infty} n^k [D_n^{*}] \tag{2}$$

$$\lambda_k = \sum_{n=1}^{\infty} n^k [R_n] \tag{3}$$

$$\xi_k = \sum_{n=1}^{\infty} (n+1)^k [Q_n] \tag{4}$$

$$\Omega_k = \sum_{m=1}^{\infty} \sum_{n=m}^{\infty} (n+m+1)^k [P_{n,m}] \qquad k = 0, 1, 2 \tag{5}$$

$$\mu_n = (\mu_1 + \mu_1^{*} + \lambda_1 + \xi_1 + \Omega_1)/(\mu_0 + \mu_0^{*} + \lambda_0 + \xi_0 + \Omega_0) \tag{6}$$

Equations for the zeroth, first and second moments of the various polymeric species are derived by summing up appropriately the equations for each of the different species separately. The smaller set of equations so obtained is given in *Table 3* (equations (3.1)–(3.11)). These moment equations alone do not comprise a *complete* set owing to the presence of terms like $[Cu^{2+}]$, $[R_1]$, $[P_{1,1}]$, $[Q_1]$, $\Sigma_{n=1}^{\infty}[P_{n,1}]$, etc., on the right-hand side. Equations for these are also incorporated in *Table 3* (equations (3.12)–(3.21)).

It may be noted from *Table 3* that the equation for $[P_{1,1}]$ includes $[Q_2]$ and $[R_2]$. We add equations for these along with those for $[D_2]$ and $[D_2^{*}]$ as equations (3.22)–(3.25). We still find five additional terms involving the $P_{n,m}$ species on the right-hand side of the 25 equations in *Table 3*. This makes the set incomplete. These terms are: $[P_{2,1}]$, $[P_{2,2}]$, $\Sigma_{n=2}^{\infty}[P_{n,2}]$, $\Sigma_{n=2}^{\infty}(n+3)[P_{n,2}]$ and $\Sigma_{n=2}^{\infty}(n+3)^2[P_{n,2}]$. If equations are written for these,

Table 2 Mass-balance equations for the various species

$$\frac{d[D_1]}{dt} = -k_1[D_1][Cu^{2+}] + k_1'[D_1^*] \tag{2.1}$$

$$\frac{d[D_n]}{dt} = -k_1[D_n][Cu^{2+}] + k_1'[D_n^*] + k_4[Q_{n-1}] \qquad n = 2, 3, \ldots \tag{2.2}$$

$$\frac{d[D_n^*]}{dt} = k_1[D_n][Cu^{2+}] - k_1'[D_n^*] = k_2[D_n^*] \qquad n = 1, 2, \ldots \tag{2.3}$$

$$\frac{d[R_1]}{dt} = k_2[D_1^*] = 2k_3[R_1]^3 = k_3[R_1]\sum_{m=2}^{\infty}[R_m] + 2k_3'[Q_1] + k_3'\sum_{m=2}^{\infty}[Q_m] = k_5[R_1]\sum_{m=2}^{\infty}[R_m] + k_5'\left([P_{1,1}] + \sum_{m=1}^{\infty}[P_{m,1}]\right) \tag{2.4}$$

$$\frac{d[R_2]}{dt} = k_2[D_2^*] = k_3[R_2][R_1] + k_3'[Q_2] = k_5[R_2][R_1] = 2k_5[R_2]\sum_{m=2}^{\infty}[R_m] + k_5'\left(\sum_{m=1}^{\infty}[P_{m,1}] + \sum_{m=2}^{\infty}[P_{m,2}] + [P_{1,1}] + [P_{2,1}] + [P_{2,2}]\right) \tag{2.5}$$

$$\frac{d[R_n]}{dt} = k_2[D_n^*] = k_3[R_n][R_1] + k_3'[Q_n] = k_5[R_n][R_1] = 2k_5[R_n]\sum_{m=2}^{\infty}[R_m] + k_5'\left([P_{n-1,n-1}] + [P_{n,n}] + \sum_{m=1}^{n-1}[P_{n-1,m}] + \sum_{m=n}^{\infty}[P_{m,n-1}] + \sum_{m=1}^{n}[P_{n,m}] + \sum_{m=n+1}^{\infty}[P_{m,n}]\right) \qquad n = 3, 4, \ldots \tag{2.6}$$

$$\frac{d[Q_1]}{dt} = k_3[R_1]^3 = k_3'[Q_1] = k_4[Q_1] \tag{2.7}$$

$$\frac{d[Q_2]}{dt} = k_3[R_1][R_2] = k_3'[Q_2] = k_4[Q_2] + 2k_6[P_{1,1}] = k_6'[Q_2] \tag{2.8}$$

$$\frac{d[Q_n]}{dt} = k_3[R_1][R_n] = k_3'[Q_n] = k_4[Q_n] + k_6[P_{n-1,1}] = k_6'[Q_n] \qquad n = 3, 4, \ldots \tag{2.9}$$

$$\frac{d[P_{1,1}]}{dt} = k_5[R_2][R_1] = 2k_5'[P_{1,1}] = 2k_6[P_{1,1}] + k_6'[Q_2] \tag{2.10}$$

$$\frac{d[P_{2,1}]}{dt} = k_5[R_3][R_1] + k_5[R_2][R_2] = 2k_5'[P_{2,1}] = 2k_6[P_{2,1}] + k_6'[Q_3] + k_6[P_{2,1}] \tag{2.11}$$

$$\frac{d[P_{3,1}]}{dt} = k_5[R_4][R_1] + k_5[R_3][R_2] = 2k_5'[P_{3,1}] = 2k_6[P_{3,1}] + k_6'[Q_4] + 2k_6[P_{2,2}] \tag{2.12}$$

$$\frac{d[P_{n,1}]}{dt} = k_5[R_{n+1}][R_1] + k_5[R_n][R_2] = 2k_5'[P_{n,1}] = 2k_6[P_{n,1}] + k_6'[Q_{n+1}] + k_6[P_{n-1,2}] \qquad n = 4, 5, \ldots \tag{2.13}$$

$$\frac{d[P_{2,2}]}{dt} = k_5[R_3][R_2] = 2k_5'[P_{2,2}] = 2k_6[P_{2,2}] + k_6[P_{3,1}] \tag{2.14}$$

$$\frac{d[P_{3,2}]}{dt} = k_5[R_4][R_2] + k_5[R_3][R_3] = 2k_5'[P_{3,2}] = k_6[P_{3,2}] + k_6[P_{4,1}] \tag{2.15}$$

$$\frac{d[P_{4,2}]}{dt} = k_5[R_5][R_2] + k_5[R_4][R_3] = 2k_5'[P_{4,2}] = 2k_6[P_{4,2}] + 2k_6[P_{3,3}] + k_6[P_{5,1}] \tag{2.16}$$

$$\frac{d[P_{n,2}]}{dt} = k_5[R_{n+1}][R_2] + k_5[R_n][R_3] = 2k_5'[P_{n,2}] = 2k_6[P_{n,2}] + k_6[P_{n-1,3}] + k_6[P_{n+1,1}] \qquad n = 5, 6, \ldots \tag{2.17}$$

For $m = 3, 4, \ldots$

$$\frac{d[P_{m,m}]}{dt} = k_5[R_{m+1}][R_m] = 2k_5'[P_{m,m}] = 2k_6[P_{m,m}] + k_6[P_{m+1,m-1}] \tag{2.18}$$

$$\frac{d[P_{m+1,m}]}{dt} = k_5[R_{m+2}][R_m] + k_5[R_{m+1}][R_{m+1}] = 2k_5'[P_{m+1,m}] = k_6[P_{m+1,m}] + k_6[P_{m+2,m-1}] \tag{2.19}$$

$$\frac{d[P_{m+2,m}]}{dt} = k_5[R_{m+3}][R_m] + k_5[R_{m+2}][R_{m+1}] = 2k_5'[P_{m+2,m}] = 2k_6[P_{m+2,m}] + 2k_6[P_{m+1,m+1}] + k_6[P_{m+3,m-1}] \tag{2.20}$$

$$\frac{d[P_{n,m}]}{dt} = k_5[R_{n+1}][R_m] + k_5[R_n][R_{m+1}] = 2k_5'[P_{n,m}] = 2k_6[P_{n,m}] + k_6[P_{n-1,m+1}] + k_6[P_{n+1,m-1}] \qquad n = m+3, m+4, \ldots \tag{2.21}$$

we find new, higher-order terms and the set of equations never gets completed. In fact, we have a hierarchy of infinite equations again, as in *Table 2*. These five terms are referred to as 'closure variables' in this paper. Closure conditions are required to break this hierarchy of equations. These are algebraic equations that express the closure variables in terms of variables on the left-hand side in the set of equations (3.1)–(3.25) of *Table 3*.

We can obtain closure conditions for polymerization systems using different amounts of insight into the nature of the process. For example, a statistical (rather than kinetic) treatment of the quinone ketal rearrangement (reaction 6) as a random-walk process could provide some guidance for the closure relations involving the species $P_{n,m}$. Fortunately, such detailed development is seldom necessary, because of the relative insensitivity of the final results (monomer conversion, number-average chain length μ_n and polydispersity index) to the *exact* equation used, *provided a small amount* of the basic character of the polymerization is reflected in the approximation. *Semi-empirical* closure conditions are, thus, quite commonly used.

Table 3 Complete set of moment (and auxiliary) equations

Moment equations

$$\frac{d\mu_m}{dt} = -k_1[Cu^{2+}]\mu_m + k_1'\mu_m^* + k_4\xi_m \qquad m = 0, 1, 2 \tag{3.1}$$

$$\frac{d\mu_m^*}{dt} = k_1[Cu^{2+}]\mu_m - k_1'\mu_m^* - k_2\mu_m^* \qquad m = 0, 1, 2 \tag{3.2}$$

$$\frac{d\lambda_0}{dt} = k_2\mu_0^* - 2k_3[R_1]\lambda_0 + 2k_3'\xi_0 - 2k_5\lambda_0(\lambda_0 - [R_1]) + 4k_5'\Omega_0 \tag{3.3}$$

$$\frac{d\lambda_1}{dt} = k_2\mu_1^* - k_3[R_1](\lambda_0 + \lambda_1) + k_3'\xi_1 - k_5\{2\lambda_0\lambda_1 - [R_1](\lambda_1 + \lambda_0)\} + 2k_5'\Omega_1 \tag{3.4}$$

$$\frac{d\lambda_2}{dt} = k_2\mu_2^* - k_3[R_1](\lambda_0 + \lambda_2) + k_3'(\xi_2 - 2\xi_1 + 2\xi_0) - k_5\{2\lambda_0\lambda_2 - [R_1](\lambda_2 + \lambda_0)\} + 2k_5'\left((\Omega_2 - \Omega_1 + \Omega_0) - 2\sum_{m=1}^{\infty}\sum_{n=m}^{\infty} nm[P_{n,m}]\right) \tag{3.5}$$

$$\frac{d\xi_0}{dt} = k_3[R_1]\lambda_0 - (k_3' + k_4 + k_6')\xi_0 + k_6\sum_{n=1}^{\infty}[P_{n,1}] + k_6[P_{1,1}] + k_6'[Q_1] \tag{3.6}$$

$$\frac{d\xi_1}{dt} = k_3[R_1](\lambda_0 + \lambda_1) - (k_3' + k_4 + k_6')\xi_1 + k_6\sum_{n=1}^{\infty}(n+2)[P_{n,1}] + 3k_6[P_{1,1}] + 2k_6'[Q_1] \tag{3.7}$$

$$\frac{d\xi_2}{dt} = k_3[R_1](\lambda_2 + 2\lambda_1 + \lambda_0) - (k_3' + k_4 + k_6')\xi_2 + k_6\sum_{n=1}^{\infty}(n+2)^2[P_{n,1}] + 9k_6[P_{1,1}] + 4k_6'[Q_1] \tag{3.8}$$

$$\frac{d\Omega_0}{dt} = k_5\lambda_0(\lambda_0 - [R_1]) - 2k_5'\Omega_0 - k_6[P_{1,1}] - k_6\sum_{n=1}^{\infty}[P_{n,1}] + k_6'(\xi_0 - [Q_1]) \tag{3.9}$$

$$\frac{d\Omega_1}{dt} = k_5\{2\lambda_0\lambda_1 - [R_1](\lambda_0 + \lambda_1)\} - 2k_5'\Omega_1 - 3k_6[P_{1,1}] - k_6\sum_{n=1}^{\infty}(n+2)[P_{n,1}] + k_6'(\xi_1 - 2[Q_1]) \tag{3.10}$$

$$\frac{d\Omega_2}{dt} = k_5\{2\lambda_0\lambda_2 + 2\lambda_1^2 - [R_1](\lambda_2 + 2\lambda_1 + \lambda_0)\} - 2k_5'\Omega_2 - 3^2k_6[P_{1,1}] - k_6\sum_{n=1}^{\infty}(n+2)^2[P_{n,1}] + k_6'(\xi_2 - 4[Q_1]) \tag{3.11}$$

Auxiliary equations

$$\frac{d[D_1]}{dt} = -k_1[D_1][Cu^{2+}] + k_1'[D_1^*] \tag{3.12}$$

$$\frac{d[D_1^*]}{dt} = k_1[D_1][Cu^{2+}] - k_1'[D_1^*] - k_2[D_1^*] \tag{3.13}$$

$$\frac{d[R_1]}{dt} = k_2[D_1^*] - k_3[R_1](\lambda_0 + [R_1]) + k_3'(\xi_0 + [Q_1]) - k_5[R_1](\lambda_0 - [R_1]) + k_5'\left([P_{1,1}] + \sum_{n=1}^{\infty}[P_{n,1}]\right) \tag{3.14}$$

$$\frac{d[Q_1]}{dt} = k_3[R_1]^2 - k_3'[Q_1] - k_4[Q_1] \tag{3.15}$$

$$\frac{d[P_{1,1}]}{dt} = k_5[R_1][R_2] - 2k_5'[P_{1,1}] - 2k_6[P_{1,1}] + k_6'[Q_2] \tag{3.16}$$

$$\frac{d}{dt}\sum_{n=1}^{\infty}[P_{n,1}] = k_5([R_1] + [R_2])(\lambda_0 - [R_1]) - 2k_5'\sum_{n=1}^{\infty}[P_{n,1}] - 2k_6\sum_{n=1}^{\infty}[P_{n,1}] + k_6\left(\sum_{n=2}^{\infty}[P_{n,2}] + [P_{2,1}] + [P_{2,2}]\right) + k_6'(\xi_0 - [Q_1]) \tag{3.17}$$

$$\frac{d}{dt}\sum_{n=1}^{\infty}(n+2)[P_{n,1}] = k_5[R_1](\lambda_0 + \lambda_1 - 2[R_1]) + k_5[R_2](\lambda_1 + 2\lambda_0 - 3[R_1]) - 2k_5'\sum_{n=1}^{\infty}(n+2)[P_{n,1}] - 2k_6\sum_{n=1}^{\infty}(n+2)[P_{n,1}] + k_6\left(\sum_{n=2}^{\infty}(n+3)[P_{n,2}] + 4[P_{2,1}] + 5[P_{2,2}]\right) + k_6'(\xi_1 - 2[Q_1]) \tag{3.18}$$

$$\frac{d}{dt}\sum_{n=1}^{\infty}(n+2)^2[P_{n,1}] = k_5[R_1](\lambda_2 + 2\lambda_1 + \lambda_0 - 4[R_1]) + k_5[R_2](\lambda_2 + 4\lambda_1 + 4\lambda_0 - 3^2[R_1]) - 2k_5'\sum_{n=1}^{\infty}(n+2)^2[P_{n,1}] - 2k_6\sum_{n=1}^{\infty}(n+2)^2[P_{n,1}] + k_6'(\xi_2 - 4[Q_1]) + k_6\left(\sum_{n=2}^{\infty}(n+3)^2[P_{n,2}] + 16[P_{2,1}] + 25[P_{2,2}]\right) \tag{3.19}$$

$$\frac{d}{dt}\sum_{m=1}^{\infty}\sum_{n=m}^{\infty} nm[P_{n,m}] = k_5\lambda_1(\lambda_1 - \lambda_0) - 2k_5'\sum_{m=1}^{\infty}\sum_{n=m}^{\infty} nm[P_{n,m}] - 2k_6\Omega_0 + k_6'(\xi_1 - 2\xi_0) \tag{3.20}$$

$$\frac{d[Cu^{2+}]}{dt} = 0.0 \tag{3.21}$$

$$\frac{d[R_2]}{dt} = k_2[D_2^*] - k_3[R_2][R_1] + k_3'[Q_2] - k_5[R_2][R_1] - 2k_5[R_2](\lambda_0 - [R_1]) + k_5'\left(\sum_{n=1}^{\infty}[P_{n,1}] + \sum_{n=2}^{\infty}[P_{n,2}] + [P_{1,1}] + [P_{2,1}] + [P_{2,2}]\right) \tag{3.22}$$

Table 3 continued

$$\frac{d[D_2^*]}{dt} = k_1[D_2][Cu^{2+}] - k_1'[D_2^*] - k_2[D_2^*] \quad (3.23)$$

$$\frac{d[D_2]}{dt} = -k_1[D_2][Cu^{2+}] + k_1'[D_2^*] + k_4[Q_1] \quad (3.24)$$

$$\frac{d[Q_2]}{dt} = k_3[R_1][R_2] - k_3'[Q_2] - k_4[Q_2] - k_6'[Q_2] + 2k_6[P_{1,1}] \quad (3.25)$$

Closure conditions

$$[P_{2,1}] = 0.38\Omega_0 f^{3.5} \quad (3.26)$$

$$[P_{2,2}] = 0.11\Omega_0 f^2 \quad (3.27)$$

$$\sum_{n=2}^{\infty}[P_{n,2}] = 0.18\Omega_0 f \quad (3.28)$$

$$\sum_{n=2}^{\infty}(n+3)[P_{n,2}] = 0.20\Omega_1 f \quad (3.29)$$

$$\sum_{n=2}^{\infty}(n+3)^2[P_{n,2}] = 0.23\Omega_2 f \quad (3.30)$$

where

$$f = \frac{\mu_0 + \Omega_0 + \lambda_0 + \mu_0^* + \xi_0}{(\mu_0 + \Omega_0 + \lambda_0 + \mu_0^* + \xi_0)_{t=0}} \quad (3.31)$$

Closure conditions similar (but not identical) to the form used for nylon-6 and poly(ethylene terephthalate)[16] did not work for the present system. We tried several other closure conditions (mostly deduced semi-empirically), before deciding upon equations (3.26)–(3.30) of *Table 3*. The coefficients and exponents in these equations have been estimated by curve-fitting data on μ_n vs. time taken from Endres and Kwiatek[8] under the following experimental conditions:

$$\text{at } t = 0$$

$$[Cu^{2+}] = 0.045\,\text{mol dm}^{-3}$$

$$\mu_k = 0.75\,\text{mol dm}^{-3} \qquad k = 0, 1, 2$$

$$\mu_k^* = \xi_k = \lambda_k = \Omega_k = 0\,\text{mol dm}^{-3} \qquad k = 0, 1, 2$$

$$[D_1] = 0.75\,\text{mol dm}^{-3} \quad (7)$$

$$[D_n] = 0\,\text{mol dm}^{-3} \qquad n = 2, 3, \ldots$$

$$[D_n^*] = [R_n] = [Q_n] = 0\,\text{mol dm}^{-3} \qquad n = 1, 2, \ldots$$

$$[P_{n,m}] = 0\,\text{mol dm}^{-3} \qquad m = 1, 2, \ldots;\ n = m, m+1, \ldots$$

More details on the development of these closure equations can be found in ref. 20.

RESULTS AND DISCUSSION

The set of moment (and other) equations (*Table 3*) corresponding to the detailed kinetic scheme can easily be integrated using Gear's method (code D02EBF in the NAG library) for stiff, ordinary differential equations (ODEs), for the initial conditions given in equations (7), and for a specified set of values of the rate constants. The initial estimates for some of these rate constants (viz. k_3, k_5, k_6, k_3', k_5', k_6') were taken from Hay *et al.*[6,7], while estimates

Table 4 Rate constants for PPO polymerization (at 27°C)

Rate constant	Initial estimates[20]	Optimal values from Box complex algorithm
k_0 (dm^3 mol^{-1} s^{-1})	0.490	0.490
k_1 (dm^3 mol^{-1} s^{-1})	0.579	0.571
k_2 (s^{-1})	1.127	1.135
k_3 (dm^3 mol^{-1} s^{-1})	4.825×10^{-4}	4.977×10^{-4}
k_4 (s^{-1})	1.930	1.839
k_5 (dm^3 mol^{-1} s^{-1})	9.165×10^2	9.25281×10^2
k_6 (s^{-1})	1.053×10^5	1.023×10^5
k_1' (s^{-1})	1.93×10^{-3}	1.781×10^{-3}
k_3' (s^{-1})	3.995×10^{-7}	4.448×10^{-7}
k_5' (s^{-1})	3.995×10^{-7}	4.065×10^{-7}
k_6' (s^{-1})	0.105	0.124

of the remaining rate constants were guessed, and then this entire set was modified slightly (tuned) till a reasonable (*visual*) fit was obtained between model predictions and the experimental data of Endres and Kwiatek[8] on μ_n vs. time. The visually 'tuned' values of the rate constants so determined are given[20] in *Table 4* (second column). We tried to improve the values of the rate constants using the more rigorous and quantitative procedure of Box[19]. The following error was minimized:

$$E = \sum_{i=1}^{N} w_i|(\mu_{n,i}^{expt} - \mu_{n,i}^{theor})|/\mu_{n,i}^{expt} \quad (8)$$

where N is the number of available data points and w_i is the weight given to the ith data point, $\mu_{n,i}^{expt}$. The theoretical values of the number-average chain length, $\mu_{n,i}^{theor}$, are calculated at the same values of t as the corresponding experimental points. The values of w_i are taken as unity for all but the last ($i = 7$) data point ($t = 840$ s). This is because the relatively larger value of the denominator makes the contribution of this term to E insignificant if its weight is the same as that for the other points. After some trial and error, we assigned a value of $w_7 = 3$ for this point. The Box complex algorithm requires a starting guess, $k_{i,start}$, for the parameters. These are taken as the values in *Table 4* (second column).

These preliminary efforts did not give as good an agreement as we expected, particularly in the initial stages of polymerization where values of μ_n are relatively low (< 5). Closer scrutiny of the experimental procedure used by Endres and Kwiatek[8] revealed that the polymer sample *actually* used for measuring μ_n experimentally would not contain much of the monomeric species, since these would be dissolved out. In order to account for this, we defined μ_n by the following modified equation:

$$\mu_n = \frac{(\mu_1 - [D_1]) + (\lambda_1 - [R_1]) + \Omega_1 + \mu_1^* + \xi_1}{(\mu_0 - [D_1]) + (\lambda_0 - [R_1]) + \Omega_0 + \mu_0^* + \xi_0} \quad (9)$$

instead of using equation (6). In equation (9), species D_1 (monomer) and R_1 are excluded from the computation of μ_n. Such a definition is more likely to reflect the actual composition of the sample used for experimental analysis than does equation (6). Use of equation (9) along with the Box complex code and initial estimates for the rate constants (*Table 4*, second column) led to best-fit (or optimal) values for the rate constants as given in the third column of *Table 4*. *Figure 1* (curve D) shows that the theoretically predicted values of μ_n using the optimal rate

constants of the third column in *Table 4* agree quite well with the experimental data of Endres and Kwiatek[8].

These rate constants were then varied to study the sensitivity of the model results to changes. This was done to explore the possibility of obtaining a simpler kinetic scheme, which would involve fewer tuning parameters. The values of the rate constants were varied by ±20% individually, and the monomer conversion, μ_n and polydispersity index (*PDI*, see 'Nomenclature') histories were studied. It was observed that the results were most sensitive to two rate constants, k_1 and k_3. Since the values of the reverse rate constants in *Table 4* (third column), k'_1, k'_3, k'_5 and k'_6, were several orders of magnitude lower than the corresponding forward rate constants, we recomputed results putting *all* the reverse rate constants as zero (i.e. assuming that the reactions were irreversible). We found that the model results were essentially unchanged. Similarly, it was observed that model predictions were not affected much when k_2 and k_4 were both made very large. On the other hand, when k_5 and k_6 were reduced to zero or made *very large*, significant changes were observed in the values of conversion, μ_n and *PDI*. Using the information generated from this sensitivity study, a simplified kinetic scheme was developed. This is given in *Table 5*. In order to maintain a resemblance with the original detailed kinetic scheme (*Table 1*), we have not renumbered the rate constants. The simplified model incorporates the very fast formation of the aryloxy radicals (R_n) from the polymeric intermediates (D_n^*). Also, the reversible reactions have been made irreversible. The model still maintains the basic step-growth *cum* chain-growth character of the original scheme, which is an important feature of this system.

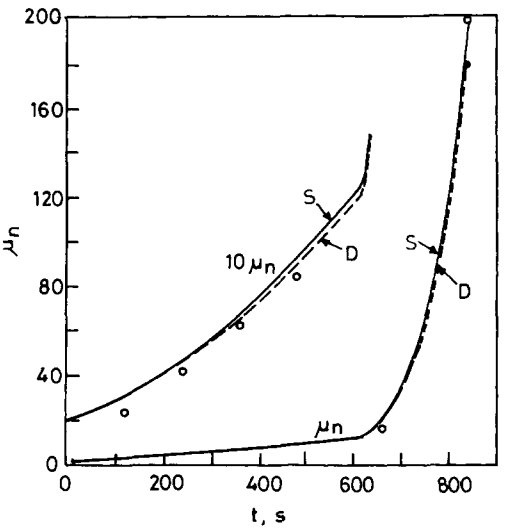

Figure 1 The μ_n history predicted using the optimal rate constants for the detailed kinetic scheme (broken curves D, obtained using optimal rate constants of *Table 4*, third column). Experimental points of Endres and Kwiatek[8] are also shown. Results using the simplified (S) model, using the rate constants of *Table 8*, are shown by full curves

Table 5 Simplified kinetic scheme for 2,6-DMP polymerization

1. $Cu^+ + \frac{1}{2}O_2 \xrightarrow{k_0} Cu^{2+}$
2. $D_n + Cu^{2+} \xrightarrow{k_1} R_n + Cu^{2+} \qquad n = 1,2,3,\ldots$
3. $R_n + R_1 \xrightarrow{k_3} D_{n+1} \qquad n = 1,2,3,\ldots$
4. $R_n + R_m \xrightarrow{k_5} P_{n,m-1}$ or $P_{n-1,m}$
   $m = 1,2,3,\ldots$
   $n = m, m+1, m+2,\ldots$
   (except $m = n = 1$)
5. $P_{n,m} \xrightarrow{k_6} P_{n+1,m-1}$ or $P_{n-1,m+1}$ all independent possibilities
6. $P_{n,1} \xrightarrow{k_6} D_{n+2} \qquad n = 1,2,3,\ldots$

The balance equations describing the variation of the concentrations of the individual species present in a (well mixed batch) reactor can easily be written for the simplified kinetic scheme of *Table 5*. These are not presented here for the sake of brevity, but can easily be deduced by simplifying the corresponding equations in *Table 2*. They can be summed up appropriately to give the moment equations. The final equations, along with the additional (auxiliary) equations that are necessary, are given in *Table 6*. We need closure equations for this case as well to break the hierarchy of equations. These are the same as those used for the detailed model, and are also included in *Table 6*. The equations given in this table form a complete set, and are integrated numerically (using the D02EBF code) for the following conditions (similar to equations (7)):

$$\begin{aligned}
&\text{at } t = 0 \\
&\mu_k = 0.75\,\text{mol dm}^{-3} \qquad k = 0,1,2 \\
&\lambda_k = 0\,\text{mol dm}^{-3} \qquad k = 0,1,2 \\
&\Omega_k = 0\,\text{mol dm}^{-3} \qquad k = 0,1,2 \\
&[D_1] = 0.75\,\text{mol dm}^{-3} \\
&[D_2] = [R_1] = [R_2] = [P_{1,1}] = 0\,\text{mol dm}^{-3} \\
&\sum_{n=1}^{\infty}[P_{n,1}] = \sum_{n=1}^{\infty}(n+2)[P_{n,1}] = \sum_{n=1}^{\infty}(n+2)^2[P_{n,1}] \\
&\qquad = 0\,\text{mol dm}^{-3} \\
&[Cu^{2+}] = 0.045\,\text{mol dm}^{-3}
\end{aligned} \tag{10}$$

Figure 2 (curve S) shows the variation of μ_n with time predicted by the simplified reaction scheme, using identical values of the rate constants (required ones from *Table 4*, third column) as used for the detailed (D) model. We find that the results are quite similar *except at large values* of t. We retune the parameters k_1, k_3, k_5 and k_6 of the simplified kinetic scheme so as to give the best quantitative fit with respect to the experimental μ_n vs. t data of Endres and Kwiatek[8]. The Box[19] complex algorithm was again used for this purpose. This algorithm minimizes the error defined in equation (8). The starting estimates of the relevant rate constants are given in *Table 4* (third column) and the ranges[21] (bounds) are given in *Table 7*. The CPU time for one such set of calculations (about 30 iterations) was about 1500 s on a Convex 220 minisupercomputer.

Figure 3 shows the variation of the error E with the iteration number for one set of choices of the algorithm parameters[21] used (see *Table 7*). We find that there is no significant reduction in the value of E beyond about 20 iterations. *Figures 4–7* show the variations of k_1, k_3, k_5

Table 6 Complete set of equations for the simplified kinetic scheme

Moment equations

$$\frac{d\mu_0}{dt} = -k_1[Cu^{2+}]\mu_0 + k_3[R_1]\lambda_0 + k_6\sum_{n=1}^{\infty}[P_{n,1}] + k_6[P_{1,1}] \tag{6.1}$$

$$\frac{d\mu_1}{dt} = -k_1[Cu^{2+}]\mu_1 + k_3[R_1](\lambda_0 + \lambda_1) + k_6\sum_{n=1}^{\infty}(n+2)[P_{n,1}] + 3k_6[P_{1,1}] \tag{6.2}$$

$$\frac{d\mu_2}{dt} = -k_1[Cu^{2+}]\mu_2 + k_3[R_1](\lambda_2 + 2\lambda_1 + \lambda_0) + k_6\sum_{n=1}^{\infty}(n+2)^2[P_{n,1}] + 9k_6[P_{1,1}] \tag{6.3}$$

$$\frac{d\lambda_0}{dt} = k_1[Cu^{2+}]\mu_0 - 2k_3[R_1]\lambda_0 - 2k_5\lambda_0(\lambda_0 - [R_1]) \tag{6.4}$$

$$\frac{d\lambda_1}{dt} = k_1[Cu^{2+}]\mu_1 - k_3[R_1](\lambda_0 + \lambda_1) - k_5\{2\lambda_0\lambda_1 - [R_1](\lambda_1 + \lambda_0)\} \tag{6.5}$$

$$\frac{d\lambda_2}{dt} = k_1[Cu^{2+}]\mu_2 - k_3[R_1](\lambda_0 + \lambda_2) - k_5\{2\lambda_0\lambda_2 - [R_1](\lambda_2 + \lambda_0)\} \tag{6.6}$$

$$\frac{d\Omega_0}{dt} = k_5\lambda_0(\lambda_0 - [R_1]) - k_6[P_{1,1}] - k_6\sum_{n=1}^{\infty}[P_{n,1}] \tag{6.7}$$

$$\frac{d\Omega_1}{dt} = k_5\{2\lambda_0\lambda_1 - [R_1](\lambda_0 + \lambda_1)\} - 3k_6[P_{1,1}] - k_6\sum_{n=1}^{\infty}(n+2)[P_{n,1}] \tag{6.8}$$

$$\frac{d\Omega_2}{dt} = k_5\{2\lambda_0\lambda_2 + 2\lambda_1^2 - [R_1](\lambda_2 + 2\lambda_1 + \lambda_0)\} - 9k_6[P_{1,1}] - k_6\sum_{n=1}^{\infty}(n+2)^2[P_{n,1}] \tag{6.9}$$

Auxiliary (additional) equations

$$\frac{d}{dt}[R_1] = k_1[D_1][Cu^{2+}] - 2k_3[R_1]^2 - k_3[R_1]\sum_{m=2}^{\infty}[R_m] - k_5[R_1](\lambda_0 - [R_1]) \tag{6.10}$$

$$\frac{d}{dt}[R_2] = k_1[D_2][Cu^{2+}] - k_3[R_2][R_1] - k_5[R_2][R_1] - 2k_5[R_2](\lambda_0 - [R_1]) \tag{6.11}$$

$$\frac{d}{dt}[D_1] = -k_1[D_1][Cu^{2+}] \tag{6.12}$$

$$\frac{d}{dt}[D_2] = -k_1[D_2][Cu^{2+}] + k_3[R_1]^2 \tag{6.13}$$

$$\frac{d}{dt}[P_{1,1}] = k_2[R_2][R_1] - 2k_6[P_{1,1}] \tag{6.14}$$

$$\frac{d}{dt}\sum_{n=1}^{\infty}[P_{n,1}] = k_5([R_1] + [R_2])(\lambda_0 - [R_1]) - 2k_6\sum_{n=1}^{\infty}[P_{n,1}] + k_6\left(\sum_{n=2}^{\infty}[P_{n,2}] + [P_{2,1}] + [P_{2,2}]\right) \tag{6.15}$$

$$\frac{d}{dt}\sum_{n=1}^{\infty}(n+2)[P_{n,1}] = k_5[R_1](\lambda_0 + \lambda_1 - 2[R_1]) + k_5[R_2](\lambda_1 + 2\lambda_0 - 3[R_1]) - 2k_6\sum_{n=1}^{\infty}(n+2)[P_{n,1}] + k_6\left(\sum_{n=2}^{\infty}(n+3)[P_{n,2}] + 4[P_{2,1}] + 5[P_{2,2}]\right) \tag{6.16}$$

$$\frac{d}{dt}\sum_{n=1}^{\infty}(n+2)^2[P_{n,1}] = k_5[R_1](\lambda_2 + 2\lambda_1 + \lambda_0 - 4[R_1]) + k_5[R_2](\lambda_2 + 4\lambda_1 - 4\lambda_0 - 3^2[R_1]) - 2k_6\sum_{n=1}^{\infty}(n+2)^2[P_{n,1}] + k_6\left(\sum_{n=2}^{\infty}(n+3)^2[P_{n,2}] + 16[P_{2,1}] + 25[P_{2,2}]\right) \tag{6.17}$$

$$\frac{d}{dt}[Cu^{2+}] = 0.0 \tag{6.18}$$

Closure conditions

$$[P_{2,1}] = 0.38\Omega_0 f^{3.5} \tag{6.19}$$

$$[P_{2,2}] = 0.11\Omega_0 f^2 \tag{6.20}$$

$$\sum_{n=2}^{\infty}[P_{n,2}] = 0.18\Omega_0 f \tag{6.21}$$

$$\sum_{n=2}^{\infty}(n+3)[P_{n,2}] = 0.20\Omega_1 f \tag{6.22}$$

$$\sum_{n=2}^{\infty}(n+3)^2[P_{n,2}] = 0.23\Omega_2 f \tag{6.23}$$

where

$$f = \frac{\mu_0 + \Omega_0 + \lambda_0}{(\mu_0 + \Omega_0 + \lambda_0)_{t=0}} \tag{6.24}$$

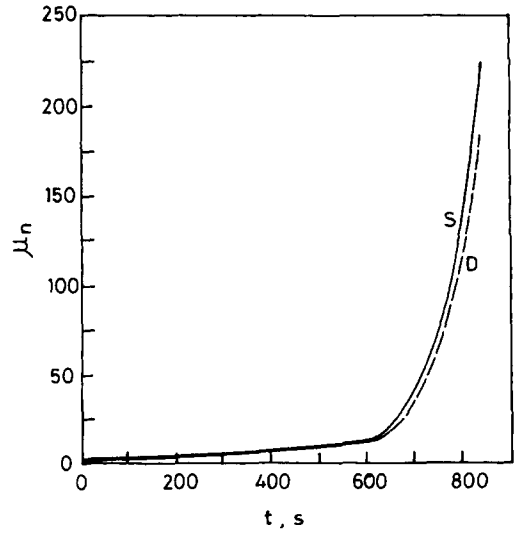

Figure 2 The μ_n vs. time histories as predicted by the simplified (S) and detailed (D) kinetic schemes using the rate constants (as required) of *Table 4* (third column)

Table 7 Parameters used for the Box algorithm (see ref. 21)

(i) $0.5 \leqslant k_i/k_{i,\text{start}} \leqslant 1.5$

$i = 1, 3, 5, 6$

($k_{i,\text{start}}$ from *Table 4*, third column)

(ii) Computational parameters for the Box complex algorithm

$\alpha = 1.3$
$\beta = 0.01$
$\gamma = 5$
$\delta = 0.0001$

Random numbers generated using G05CBF and G05DAF subroutines of the NAG library

and k_6 with the iteration number, as the best-fit values are attained. It can be seen that the values of k_1 and k_3 have stabilized at about 30 iterations, about the same as where the error E has stabilized. On the other hand, the values of k_5 and k_6 have not stabilized, and continue to vary somewhat erratically. Since the values of μ_n are far more sensitive to k_1 and k_3 than to k_5 and k_6, we take the values of the latter two rate constants at iteration number 30 as the best-fit values. The four best-fit values are given in *Table 8*. It may be added that two of the rate constants change with iteration number in a somewhat correlated manner. This is purely a coincidence, and such correlations would vanish with a different choice of the initial (guess) solution.

Figure 1 shows the variation of μ_n with time as predicted by the simplified (S) model using these best-fit values. We see that the number-average chain-length history predicted by the simplified model compares favourably with the experimental data[8]. In fact, it shows a slightly better agreement at the high-molecular-weight end than the detailed (D) kinetic model with the optimal rate constants of *Table 4* (third column). We recommend the use of the simplified model for simulation work.

Figures 8 and *9* show the variation of monomer concentration and the *overall PDI* (see 'Nomenclature' for exact definition) of the polymer formed, using the best-fit values of the rate constants in the simplified kinetic model (curves indicated by 0). Unfortunately, Endres and Kwiatek[8] do not report experimental results for these important quantities. It is observed that the monomer, D_1, depletes fairly rapidly (to low-molecular-weight species), even though high values of μ_n are attained much later. This is typical of step-growth polymerization, and is a consequence of the special kinetic scheme associated with PPO polymerization, in which both chain-growth and step-growth characteristics are present. The *PDI* plot in *Figure 9* shows a decrease in the *PDI* after $t \sim 425$ s (point C), and an increase again with t after about 600 s (point D). Detailed studies[20] of the μ_n and *PDI* of the *individual* species (R_n, D_n and $P_{n,m}$) have been made to explain the unusual behaviour

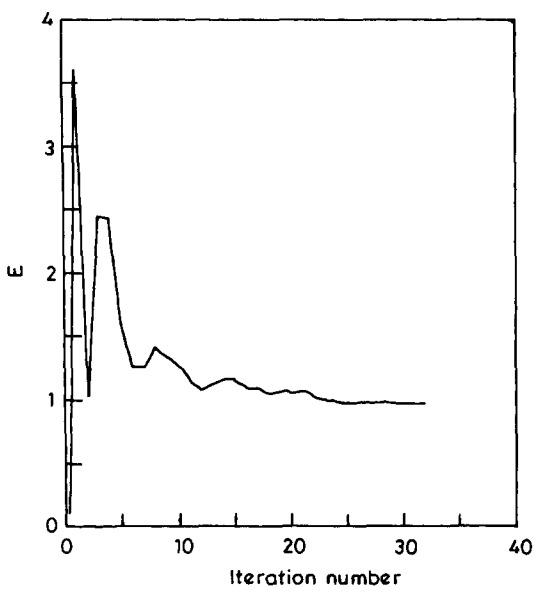

Figure 3 Variation of error E with iteration number during optimization by the Box complex algorithm

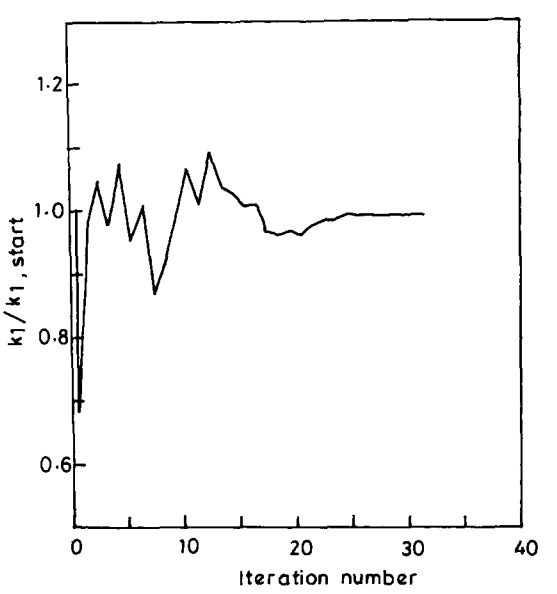

Figure 4 Variation of $k_1/k_{1,\text{start}}$ with iteration number during optimization by the algorithm of Box

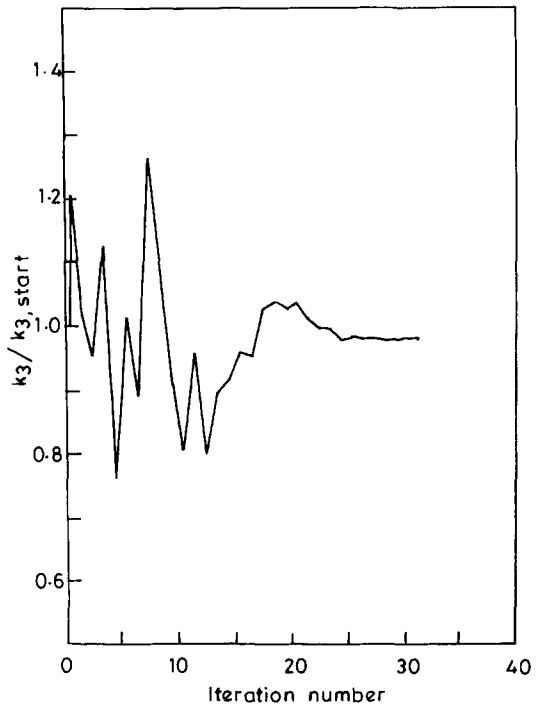

Figure 5 Variation of $k_3/k_{3,start}$ with iteration number during optimization by the algorithm of Box

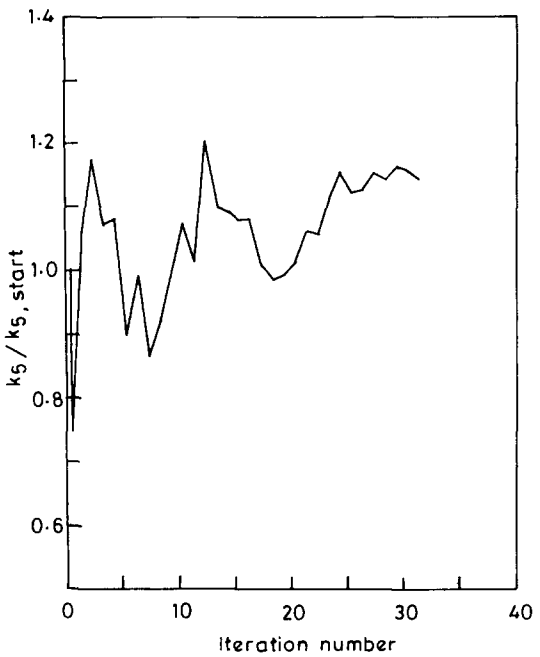

Figure 6 Variation of $k_5/k_{5,start}$ with iteration number during optimization by the algorithm of Box

of the *PDI* of the *overall* polymer. It is found that the overall *PDI* increases during 100 s $< t <$ 425 s (path BC) because of mixing of large (but decreasing) amounts of R_1 (higher R_n are almost absent) with almost equal amounts of D_n, whose chain length increases with time. Thereafter (for 425 s $< t <$ 600 s; path CD) the amount of R_1 becomes negligible, and the overall *PDI* is determined primarily by the *PDI* of the D_n species alone, and this decreases with time. The increase of the

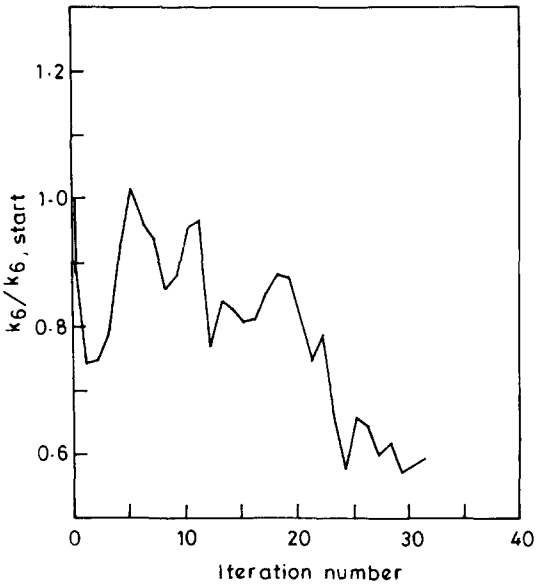

Figure 7 Variation of $k_6/k_{6,start}$ with iteration number during optimization by the algorithm of Box

Table 8 Best-fit values for the parameters of the simplified kinetic scheme

$k_1 = 0.568\,dm^3\,mol^{-1}\,s^{-1}$
$k_3 = 4.855 \times 10^{-4}\,dm^3\,mol^{-1}\,s^{-1}$
$k_5 = 10.74899 \times 10^2\,dm^3\,mol^{-1}\,s^{-1}$
$k_6 = 0.5854 \times 10^5\,s^{-1}$
Value of E at iteration number 30 is 0.967 788

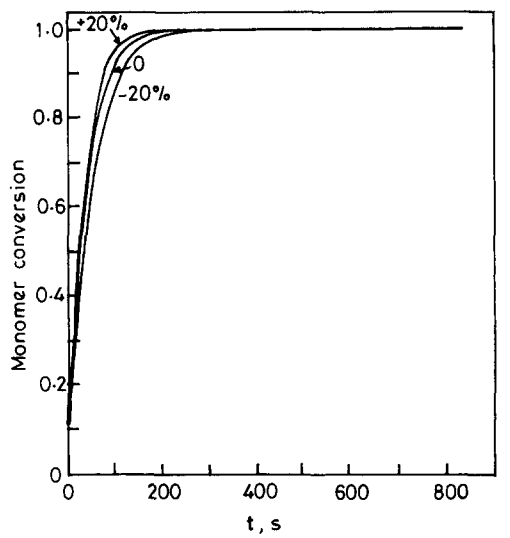

Figure 8 Sensitivity of monomer conversion history to k_1 for the simplified model. All other rate constants are at the values given in *Table 8*

overall *PDI* after $t \sim$ 600 s (path DE) is associated with larger amounts of high-chain-length $P_{n,m}$ species, which get formed after this time.

A detailed sensitivity study is now carried out for the simplified model. This gives some (qualitative) idea of the effect of temperature on the μ_n history, since experimental

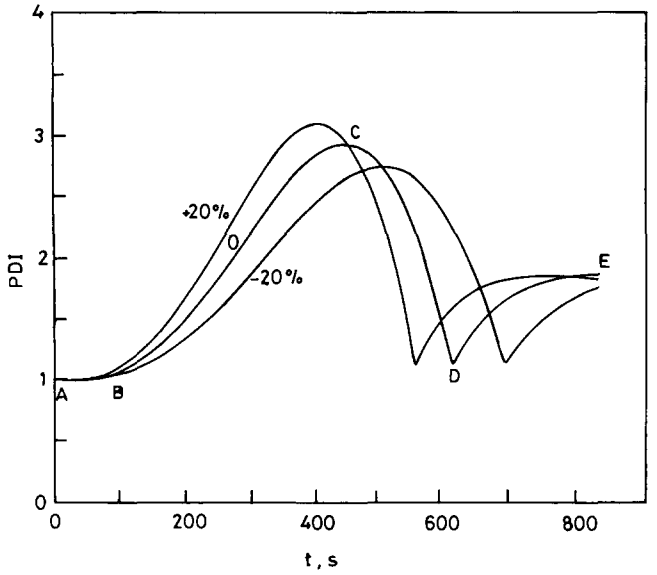

Figure 9 Sensitivity of $PDI\,(t)$ to k_1 for the simplified model. All other rate constants are at the values given in *Table 8*

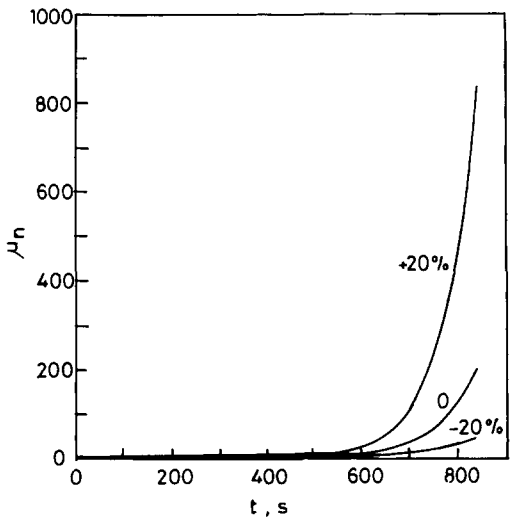

Figure 10 Sensitivity of $\mu_n(t)$ to k_1 for the simplified model. All other rate constants are at the values given in *Table 8*

results on the activation energies of the rate constants are not available in the open literature. The rate constants are varied by ±20% individually around the values in *Table 8*. *Figures 8–10* show the results corresponding to changes in k_1. Significant changes, particularly in the final values of μ_n, are observed as k_1 is changed. The value of μ_n rises to as high as 900 for a 20% increase in k_1. This stresses the need for good temperature control of the reactor, as well as for a good estimate of this rate constant using more (and as yet unavailable) experimental data. The final value of the *PDI* is not significantly altered, nor is the final value of the monomer conversion—both of interest to a reactor engineer. The higher rate of conversion corresponding to higher values of k_1 is as expected.

Figures 11 and *12* show similar effects associated with the variation of k_3. In this case also, μ_n rises to significantly higher values, though not as much as in

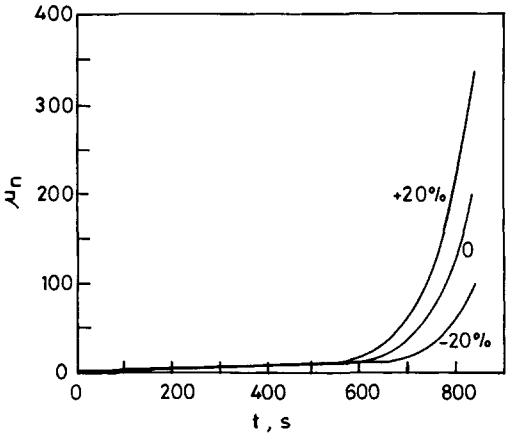

Figure 11 Sensitivity of $\mu_n(t)$ to k_3 for the simplified model. All other rate constants are at the values given in *Table 8*

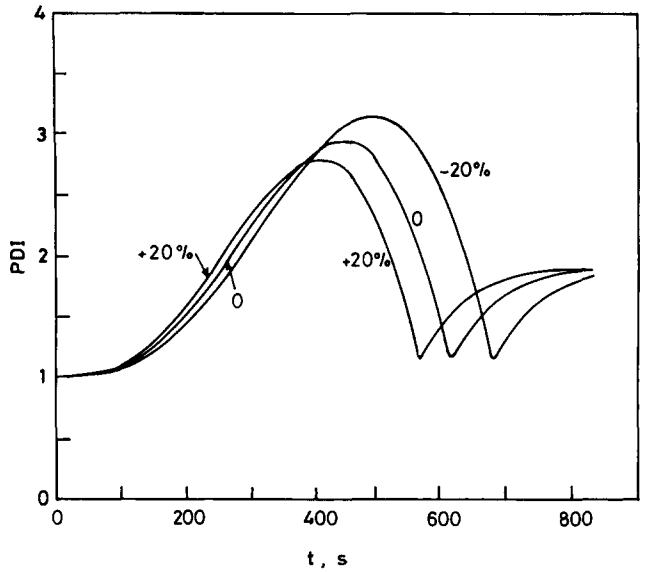

Figure 12 Sensitivity of $PDI(t)$ to k_3 for the simplified model. All other rate constants are at the values given in *Table 8*

Figure 10, by a 20% increase in k_3. This is expected because a larger value of k_3 leads to an early end of the chain-growth phase of the reaction by depleting R_1 at a higher rate. This leads to higher concentrations of long molecules in the reaction mass, which triggers the step-growth phase. The behaviour of the *PDI* history, on the other hand, is in complete contrast to that observed in *Figure 9*. The peak is higher for lower values of k_3. This is because lower values of k_3 prolong the presence of R_1 in the reaction mass, while higher-chain-length D_n species are formed. This leads to higher dispersity in the macromolecular system, which, in turn, leads to higher values of the *PDI*.

When k_5 and k_6 are varied by ±20%, it is observed that there is relatively little change in the histories of monomer conversion, μ_n and *PDI*. The change in the values of μ_n, *PDI* and monomer conversion at $t = 840$ s for this situation is given in *Table 9*. The model results are, thus, relatively insensitive to *small* changes in these two rate constants. In view of this, one could as well have used the initial (guess) values of k_5 and k_6 (*Table 4*, third column), though we recommend the use of the values suggested by the Box algorithm, which give slightly

Table 9 Variation of monomer conversion, μ_n and *PDI* at $t = 850$ s associated with changes of ±20% in k_5 and k_6

Rate constant changed	Amount changed	Monomer conversion	μ_n	*PDI*
–	0% (reference)	1.0	200.0	1.876
k_5	+20%	1.0	201.285	1.882
k_5	−20%	1.0	198.270	1.869
k_6	+20%	1.0	200.0	1.876
k_6	−20%	1.0	200.0	1.876

improved results. The reactions with which k_5 and k_6 are associated cannot be eliminated from the simplified kinetic scheme since these would eliminate the crucial intermediate species, $P_{n,m'}$ which are really responsible (as demonstrated in ref. 20) for the sudden increase in the value of μ_n beyond $t \sim 600$ s, and lend a step-growth character to the polymerization. *Large* variations of k_6 do, indeed, lead to changes in the results. In view of this, it would be inappropriate to eliminate k_6 and replace reactions 4–6 of *Table 5* by:

$$R_n + R_m \xrightarrow{k_5} D_{n+m} \qquad (11)$$

even though using equation (11)with a retuned set of rate constants k_1, k_3 and k_5 could fit the *single* available set of $\mu_n(t)$ data equally well. Indeed there is a (small) likelihood that we may have to give up the simplified model of *Table 5* and use the fundamentally sound and more detailed kinetic scheme of *Table 1*, if future experimental data point towards that direction.

CONCLUSIONS

A simplified, four-parameter kinetic scheme is developed for the production of poly(phenylene oxide). The μ_n, *PDI* and monomer conversion histories predicted by this model are found to give results that are in reasonable agreement with those predicted by the more detailed model, as well as with some experimental data on $\mu_n(t)$. The new model involves the use of only four parameters, of which only two need to be estimated accurately. Optimal values of these parameters are obtained so as to minimize the weighted sum of normalized errors with respect to some experimental μ_n vs. t data. This simple kinetic model can now be used to simulate, optimize or control industrial PPO reactors.

ACKNOWLEDGEMENT

The authors would like to thank the reviewer of this paper for several very perceptive and knowledgeable comments.

NOMENCLATURE

D_n polymer molecule with n repeat units
D_n^* polymeric intermediate with n repeat units
E error (equation (8))
f ratio of total number of molecules (all species) to the number of molecules present initially
k_i rate constants for forward reactions ($dm^3\ mol^{-1}\ s^{-1}$ or s^{-1})
k_i' rate constants for reverse reactions ($dm^3\ mol^{-1}\ s^{-1}$ or s^{-1})
$P_{n,m}$ quinone ketal molecule with n repeat units on the left of the cyclohexadiene group and m repeat units on the right
PDI polydispersity index ($\equiv \alpha_0\alpha_2/\alpha_1^2$) of the entire macromolecular species
Q_n quinol ether molecule with $(n+1)$ repeat units
R_n polymeric aryloxy radical with n repeat units
t time (s)
w weight factor in the error E

α_k sum of kth moments of all macromolecular species ($= \mu_k + \mu_k^* + \lambda_k + \xi_k + \Omega_k$, or $\mu_k + \lambda_k + \Omega_k$); $k = 0, 1, 2$ ($mol\ dm^{-3}$).
λ_k kth moment of R species; $k = 0, 1, 2$ ($mol\ dm^{-3}$)
μ_k kth moment of D species; $k = 0, 1, 2$ ($mol\ dm^{-3}$)
μ_k^* kth moment of D^* species; $k = 0, 1, 2$ ($mol\ dm^{-3}$)
μ_n number-average chain length of the entire macromolecular species ($\equiv \alpha_1/\alpha_0$ or as in equation (9))
ξ_k kth moment of Q species ($mol\ dm^{-3}$)
Ω_k kth moment of P species ($mol\ dm^{-3}$)

[ ] molar concentration ($mol\ dm^{-3}$)

REFERENCES

1 Karasz, F. E. and O'Reilly, J. M. *J. Polym. Sci., Polym. Lett. Edn.* 1965, **3,** 561
2 Heijboer, J. *J. Polym. Sci. (C)* 1968, **16,** 3755
3 Aycock, D., Abolins, V. and White, D.M. in 'Encyclopedia of Polymer Science and Engineering' (Eds. H. F. Mark, N. M. Bikales, C. G. Overberger, G. Menges and J. I. Kroschwitz), Vol. 13, 2nd Edn., Wiley, New York, 1988, pp. 1–30
4 Hay, A. S., Shenian, P., Gowan, A. C., Erhardt, P. F., Haaf, W. R. and Theberge, J. E. in 'Encyclopedia of Polymer Science and Technology' (Eds. H. F. Mark, N. G. Gaylord and N. M. Bikales), Vol. 10, 1st Edn., Interscience, New York, 1969, pp. 92–111
5 White, D. M. in 'Comprehensive Polymer Science', Vol. 5, 'Step Polymerisation' (Eds. G. C. Eastmond, A. Ledwith, S. Russo and P. Sigwalt), Pergamon, Oxford, 1989, pp. 473–481
6 Hay, A. S., Blanchard, H. S., Endres, G. F. and Eustance, J. W. *J. Am. Chem. Soc.* 1959, **81,** 6335
7 Hay, A. S. *J. Polym. Sci.* 1962, **58,** 581
8 Endres, G. F. and Kwiatek, J. *J. Polym. Sci.* 1962, **58,** 593
9 Endres, G. F., Hay, A. S. and Eustance, J. W. *J. Org. Chem.* 1963, **28,** 1300
10 Finkbeiner, H., Hay, A. S., Blanchard, H. S. and Endres, G. F. *J. Org. Chem.* 1966, **31,** 549
11 McNelis, F. M. *J. Org. Chem.* 1966, **31,** 1255
12 Tsuchida, E., Kaneko, M. and Nishide, H. *Makromol. Chem.* 1972, **151,** 221
13 Mobley, D. P. *J. Polym. Sci., Polym. Chem. Edn.* 1984, **22,** 3203
14 Koning, C. E., Brinkhuis, R. and Challa, G. *Polymer* 1987, **28,** 2310
15 Chen, W. and Challa, G. *Polymer* 1990, **31,** 2171
16 Gupta, S. K. and Kumar, A. 'Reaction Engineering of Step Growth Polymerisation', Plenum, New York, 1987
17 Ray, W. H. *J. Macromol. Sci., Rev. Macromol. Chem. (C)* 1972, **8,** 1
18 Gupta, S. K., Kumar, A. and Krishnamurty, M. V. G. *Polym. Eng. Sci.* 1985, **25,** 37
19 Box, M. *Comput. J.* 1965, **8,** 42
20 Kuberkar, S. T. and Gupta, S. K. *J. Polym. Eng.* 1995, **15,** 243
21 Ravi Kumar, V. and Gupta, S. K. *Polymer* 1991, **32,** 3233